Published version available at: https://doi.org/10.1016/j.proci.2022.07.065

Flame propagation in narrow horizontal channels: impact of the gravity field on the flame shape

Anne Dejoan[a], Carmen Jiménez[a], Daniel Martínez-Ruiz[b], Victor Muntean[b], Mario Sánchez-Sanz[c], Vadim N. Kurdyumov [a,*]

[a] *Energy Department, CIEMAT, Madrid, Spain*
[b] *ETSIAE, Universidad Politécnica de Madrid, Madrid, Spain*
[c] *Universidad Carlos III de Madrid, Leganés, Spain*

Abstract

In this paper, we study the effect of gravity, or buoyancy forces, on the structure of flames propagating in horizontal channels. It is shown that there are two mechanisms for the appearance of non-symmetric flames. The first, more obvious, is related to buoyancy, when a hotter gas of lower density tends to be located in the upper half of the channel. However, there is a second mechanism associated with the intrinsic flame instabilities, which also can cause the loss of flame symmetry. This mechanism can, at certain values of the parameters, act in the opposite direction, when hotter gases are enclosed in the lower part of the channel. In this case, two stable non-symmetric solutions may exist in the presence of gravitational forces and the establishment of one or another configuration depends on the initial conditions. The stability of these solutions is demonstrated by time-dependent computations.

Keywords: Narrow channel; Premixed laminar flame propagation; Non-symmetric flames; Buoyancy forces; . . . (8/10)

1. Introduction

The first pioneering numerical studies on premixed flames freely propagating in channels can be traced back more than thirty years [1, 2]. In later years, research on this topic has multiplied, due to its importance for the design of many combustion devices and their safe operation [3–9].

It should be noted that in most of the early studies on freely propagating flames, a condition of flame symmetry about the middle of the channel (or its axis for circular channels) was applied to reduce computational costs, so the non-symmetric flames were not captured. Perhaps the first investigations where this limitation was not imposed were those reported in [5, 9].

When a premixed flame propagates in a channel, its speed depends on the flame surface area in which the combustion process takes place. For this reason, the shape of the flame is of great importance in propagation properties and there is significant amount of works exploring this issue. There are quite a number of effects that determine the flame shape. First of all, such effects as heat losses [3, 10–13], the effect of the Lewis number [5, 13–19], the influence of the flow rate [5, 9, 14, 17], thermal expansion [13, 18] and others should be mentioned. Among the latter are the buoyancy forces, which were recently considered in [20] for flames stabilized with respect to the channel walls.

Under experimental conditions, the study of flame propagation is often carried out in channels situated horizontally. In these cases, a natural question arises of how the buoyancy forces generated by changes in the gas density affect the structure and dynamics of the flame. It would be logical to assume at first glance that the buoyancy forces could break the symmetry of the flame relative to the middle of the channel, which could occur in their absence, leading to the hotter gas to be located preferentially in the upper half of the channel. On the other hand, as was shown recently in numerical simulations for channels of sufficient width, e.g see [13], the flame may also become nonsymmetric by itself and without the participation of buoyancy. This effect is a manifestation of intrinsic flame instabilities: diffusive-thermal instability and hydrodynamic Darrieus-Landau instability. When these instabilities break the flame symmetry in the absence of a gravity field, it is obvious that two non-symmetric flame configurations, mirrored relative to the mid-channel, are possible. These two configurations are stable in the absence of gravity, in contrast to the symmetric solution, which, although it exists as a mathematical object, becomes unstable. The aim of this work is to try to answer the question of how buoyancy forces will affect this situation.

It should be noted that this work is not aimed at building a complete map of possible solutions nor at performing an exhaustive parametric analysis. Contrarily, it is rather intended to highlight the most significant details affecting the shape of the flame, while excluding secondary effects, as it seems to the authors. For this purpose, we consider only planar channels with adiabatic walls, excluding heat losses from consideration, and we study only lean mixtures (where the oxidant concentration remains approximately constant) using one-step Arrhenius kinetics. The results obtained by relaxing these assumptions will be reported elsewhere.

The work is structured as follows. Section 2 proposes a mathematical formulation of the problem. Section 3 describes the solution methods. Section 4 presents the numerical results obtained on the basis of steady-state solutions, which are then confirmed by time-dependent calculations. The last section offers a discussion of the results.

2. General formulation

Consider a lean combustible mixture (fuel and oxidizer) at initial temperature T_0, density ρ_0 and fuel mass fraction Y_0, flowing with mean velocity U_0 in a horizontal channel of height h. For the sake of simplicity, we consider planar adiabatic two-dimensional channels. In what follows, x', y' denote the longitudinal and wall-normal coordinates, respectively. The influence of the third coordinate z', transverse to the motion of the mixture, will be neglected. The results of modeling three-dimensional flames require significantly large numerical costs and will be reported elsewhere. Primes here and hereafter mark dimensional quantities if the same notation is used for dimensional and non-dimensional variables. The subindex "0" indicates initial fresh gas stream values.

The combustible mixture undergoes a chemical reaction modeled by a global irreversible step $F+O \rightarrow P$, where F denotes the fuel, O the oxidizer and P the products. Assuming that the mixture is lean in fuel, the oxidizer mass fraction remains nearly constant. The amount of fuel consumed per unit volume and per unit time is given by $\Omega = \mathcal{B}\rho^2 Y \exp\left(-\mathcal{E}/\mathcal{R}_g T\right)$, where $\mathcal{B}$ is a pre-exponential factor containing the molecular weights of fuel and oxidizer molecules, ρ is the density of the mixture, Y is the fuel mass fraction, $\mathcal{E}$ is the overall activation energy and $\mathcal{R}_g$ is the universal gas constant. We assume also constant transport properties and heat capacity c_p of the mixture.

The burning velocity of the planar flame S_L, the thermal flame thickness defined as $\delta_T = \mathcal{D}_T/S_L$, with $\mathcal{D}_T = \lambda_g/\rho_0 c_p$ the thermal diffusivity, and the adiabatic flame temperature $T_a = T_0 + QY_0/c_p$, with Q the total heat of combustion per unit mass of fuel, are used below to specify the non-dimensional parameters. Using the above scales based on the flame properties allows to compare numerical results calculated for different chemical and transport parameters. To this end, the dimensionless channel height, $a = h/\delta_T$, and the dimensionless flow rate, $m = U_0/S_L$, are introduced.

Dimensionless variables are defined as follows

$$\begin{gathered} t = t' S_L/\delta_T,\ x = x'/\delta_T,\ y = y'/h, \\ u = u'/S_L,\ v = v'/(aS_L), \\ \rho = \rho'/\rho_0,\ Y = Y'/Y_0, \\ \theta = (T - T_0)/(T_a - T_0),\ p = a^2 p'/\rho_0 S_L^2, \end{gathered} \tag{1}$$

where u, v denote the velocity components in the x- and y-directions, respectively, and p is the pressure.

For the steady-state solutions reported below (obtained by imposing $\partial/\partial t = 0$ in the governing equations), the reference frame was attached to the flame, namely to a point (x_*, y_*) with a given temperature $\theta = \theta_*$. The velocity of this point with respect to the wall, $u_f = U_f/S_L$, constitutes an eigenvalue of the problem and gives the flame propagation velocity. Indeed, in the case of steady flame propagation the whole flame surface propagates with a constant velocity equal to u_f, which is independent of both the location of the reference point and of the reference temperature. Evidently, θ_* and y_* must be chosen judiciously so that this point lies outside the quenching layer near the wall (if it exists in non-adiabatic scenarios). Calculations of time-dependent flame dynamics were also carried out where a reference frame attached to the wall was used. In this case $u_f = 0$ was imposed in the governing equations presented below. Notice that in both cases u and v represent the flow velocities with respect to the wall and there are no non-inertial forces in the momentum conservation equation.

Under the above and zero-Mach number assumptions, the governing equations and the equation of state are

$$\begin{gathered} \rho_t + (\rho[u + u_f])_x + (\rho v)_y = 0, \\ \rho(u_t + [u + u_f]u_x + v u_y) = -a^{-2} p_x \\ + Pr\,[a^{-2} u_{yy} + \tfrac{4}{3} u_{xx} + \tfrac{1}{3} v_{xy}], \\ \rho(v_t + [u + u_f]v_x + v v_y) = -a^{-4} p_y \\ + Pr\,[a^{-2}(\tfrac{4}{3} v_{yy} + \tfrac{1}{3} u_{xy}) + v_{xx}] - \rho G, \\ \rho(\theta_t + [u + u_f]\theta_x + v\theta_y) = \\ \theta_{xx} + a^{-2}\theta_{yy} + \omega, \\ \rho(Y_t + [u + u_f]Y_x + v Y_y) = \\ Le^{-1}[Y_{xx} + a^{-2} Y_{yy}] - \omega, \\ \rho(1 + q\theta) = 1, \end{gathered} \tag{2}$$

where subscripts denote partial differentiation. The reaction rate term takes the form

$$\omega = \frac{\beta^2 (1+q)^2}{2 Le u_p^2} \rho^2 Y \exp\left\{ \frac{\beta(\theta - 1)}{(1 + q\theta)/(1+q)} \right\}, \tag{3}$$

In addition to the parameters $a = h/\delta_T$ and $m = U_0/S_L$, the following dimensionless groups appear in Eqs. (2)-(3)

$$\begin{gathered} q = \frac{(T_a - T_0)}{T_0},\ Pr = \frac{\mu c_p}{\lambda_g},\ Le = \frac{\lambda_g}{\rho_0 c_p \mathcal{D}}, \\ \beta = \frac{\mathcal{E}(T_a - T_0)}{\mathcal{R}_g T_a^2},\ G = \frac{g\delta_T}{S_L^2}, \end{gathered} \tag{4}$$

representing the conventional heat release, Prandtl, Lewis, Zel'dovich and gravity parameters, respectively, with μ and $\mathcal{D}$ the viscosity and mass (fuel) diffusivity. In what follows, the values $Pr = 0.7$, $\beta = 10$ and $q = 5$ were fixed in all cases presented. The main goal of this work is to study the effect of the gravity parameter G, the dimensionless width a and the flow rate m on the flame structure.

The no-flux and no-slip conditions applied at the wall take the form

$$y = 0, 1: \quad \theta_y = Y_y = u = v = 0\,. \tag{5}$$

Since axial diffusion becomes negligible far upstream the flame, the state of the gas is constant and uniform with $v = 0$. The flow field is unidirectional and satisfies the equations $p_y = 0$ and $p_x = Pr \cdot u_{yy}$. As a result, a Poiseuille flow determined by the mean flow rate m is established with

$$\begin{gathered} u = 6m\, y(1 - y), \quad v = \theta = Y - 1 = 0, \\ \text{as} \quad x \to -\infty\,. \end{gathered} \tag{6}$$

For far downstream boundary condition we require

$$\begin{gathered} \theta_{xx} = Y_{xx} = u_x = v = 0, \\ \text{as} \quad x \to +\infty. \end{gathered} \tag{7}$$

This weak outlet boundary condition for the temperature field replaces a more severe zero-temperature condition which should be imposed far downstream when heat losses are not negligible. The conditions for the gas velocity correspond to a downstream flow parallel to the wall. These conditions are less restrictive than those explicitly specifying particular distributions of variables. The numerical simulations reported below show that the influence of the downstream boundary condition becomes negligible, as it should be, if the size of the computational domain is reasonably long downstream the flame.

The factor $u_p = S_L/S_L^{as}$ included in Eq. (3) ensures that the non-dimensional speed of a planar adiabatic flame equals one for a given finite β, where S_L^{as} is the asymptotic value of adiabatic planar flame speed calculated at $\beta \to \infty$:

$$S_L^{as} = \sqrt{2(\lambda_0/c_p) Le \beta^{-2} \mathcal{B}}(T_0/T_a) e^{-\mathcal{E}/2\mathcal{R}T_a}\,. \tag{8}$$

For the parameter values $\beta = 10$ and $q = 5$ used in this study, the value of this factor is $u_p = 1.0547$ for $Le = 1$ and $u_p = 1.0746$ for $Le = 0.8$, the cases explored in the present study.

3. Numerical treatment

Steady-state computations were carried out in a finite domain, $x_{min} \le x \le x_{max}$, using $x_{min} = -20$ and $x_{max} = 20$ as typical values. All the steady-state numerical results reported below were obtained using second-order, three-points central differences for spatial derivatives on a rectangular uniform grid. Typical values for the non-dimensional reference temperature

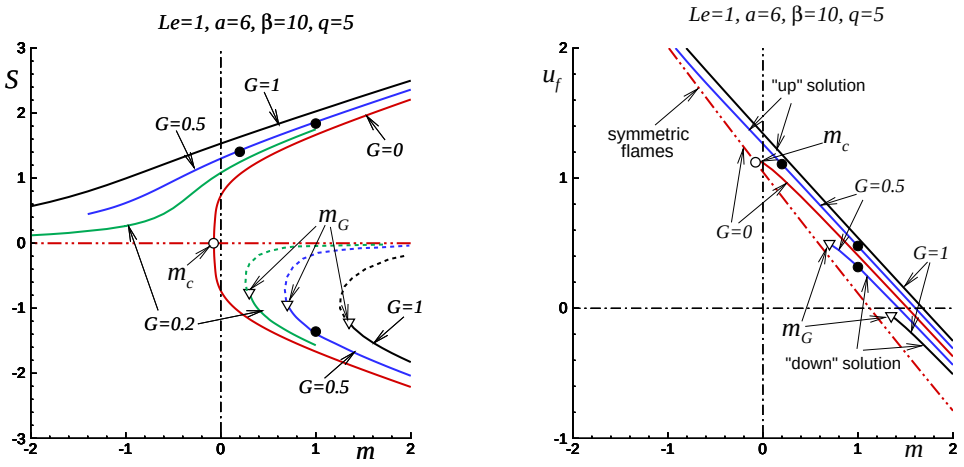

Fig. 1: Symmetry index S (left plot, for $G = 0$, 0.2, 0.5 and 1) and flame velocity relative to the channel walls u_f (right plot, for $G = 0$, 0.5 and 1) as functions of flow rate m; all curves for $a = 6$, $Le = 1$, $\beta = 10$ and $q = 5$. The dash-dot-dot curve shows the symmetrical solution computed in a half-width domain. The dashed lines in the left plot show the intermediate (not calculated) branch of the solution, which is generated from the symmetric solution at $G > 0$. The filled circles in both plots indicate the final solutions obtained by the time-dependent method. The critical value m_c (for $G = 0$) is shown by an open circle, the critical values m_G are shown by open triangles.

were $\theta_* = 0.5 \div 0.7$. The reference point was located at $y_* \approx 0.5 \div 0.9$ and approximately in the middle of the domain along the x-axis. The independence of the results to these values was verified specifically.

The stream function-vorticity formulation was adopted for the steady-state computations. With the stream function ψ, defined from

$$\rho(u + u_f) = \psi_y, \quad \rho v = -\psi_x \,, \tag{9}$$

and the vorticity $\zeta = a^2 v_x - u_y$, the Navier-Stokes equations reduce to

$$\rho([u + u_f]\zeta_x + v\zeta_y) = Pr[\zeta_{xx} + a^{-2}\zeta_{yy}] - Ga^2\rho_x + J \,, \tag{10}$$

$$a^2(\psi_x/\rho)_x + (\psi_y/\rho)_y = -\zeta \tag{11}$$

where J is the vorticity production given by

$$J = (\rho[u + u_f])_y u_x - a^2(\rho[u + u_f])_x v_x + (\rho v)_y u_y - a^2(\rho v)_x v_y \,.$$

Equations (9)-(11) along with the boundary conditions (properly rewritten in terms of ψ and ζ) were solved numerically using a Gauss-Seidel iteration method with successive over-relaxation to determine the eigenvalue u_f.

In order to study the effect of buoyancy forces, symmetric solutions were also calculated for $G = 0$ separately by reducing the domain to half its width, $0 \le y \le 1/2$, and imposing symmetric boundary conditions for the temperature, the mass fraction and the velocities at the centerline, namely

$$y = 1/2: \quad \theta_y = Y_y = u_y = v = 0. \tag{12}$$

In order to determine the quantitative degree of asymmetry of the obtained solution, the following integral was calculated

$$S = \int_{-\infty}^{\infty} dx \int_0^{1/2} [\theta(x, y, t) - \theta(x, 1 - y, t)] dy \,. \tag{13}$$

Clearly, $S = 0$ (within numerical accuracy) for a symmetric solution, and takes non-zero values when the solution becomes non-symmetric with respect to the horizontal $y = 1/2$ axis.

For the unsteady calculations presented below, the set of dimensionless time-dependent equations (2) was resolved imposing $u_f = 0$. Two different numerical procedures were used. In the first one, unsteady simulations were carried out using a compressible Navier-Stokes solver described in [21], with 6th-order finite differences and 3d order Runge-Kutta time-integration. We adopted a reference frame moving with the flame, by measuring iteratively the flame propagation speed, as $u_f = \int_{-\infty}^{\infty} \int_0^1 \omega dx dy - m$, and making the coordinate system move with this velocity, as done in [16]. In another numerical procedure the unsteady calculations were performed making use of the open source code OpenFOAM [22]. For temporal discretization, the first order Euler scheme was

used with second-order cell center scheme for spatial discretization. Both methods of calculations gave very similar results.

4. Results

4.1. Steady-state solutions for $Le = 1$

This study does not examine the flame structure for a specific fuel/air mixture. However, it is easy to estimate that the gravitational parameter $G = g\delta_T/S_L^2 = g\mathcal{D}_T/S_L^3$, which is formally equal to the inverse Froude number based on the speed and thermal thickness of the corresponding planar flame, can take values slightly less than, or even of the order of, unity for lean mixtures. Indeed, this happens at planar flame speeds smaller than $10\,cm/s$, for example.

Fig. 1 shows the steady-state numerical results for the symmetry index, S (left plot), and the flame velocity relative to the channel walls, u_f (right plot), plotted as a function of the flow rate m for $a = 6$, $Le = 1$ and varying G. As shown in [13] for $G = 0$, two non-symmetric flame solutions appear for a fairly wide channel when the flow rate exceeds a certain critical value, m_c. These solutions have nonzero and opposite values of the symmetry index S. In addition to these two solutions mirrored with respect to the middle of the channel, a symmetric unstable solution (corresponding to the curve with $S = 0$) also exists for $m > m_c$. For $m < m_c$, this symmetric solution is unique and stable. Despite the fact that the symmetric solution is unstable for $m > m_c$, it is easily obtained in calculations where only half of the channel width is considered applying the symmetry conditions given by Eq. (12). The curves corresponding to the symmetric solutions are drawn by dash-dot-dot lines in Fig. 1.

For the $a = 6$ case shown in Fig. 1, this critical value for the flow rate above which two non-symmetric solutions appear is $m_c \approx -0.0756$, in the absence of buoyancy. This point is marked by an open circle in the figure on the curve with $G = 0$. For convenience, we will identify the non-symmetric solutions as "up" and "down" solutions when the hotter gas is located in the upper ($S > 0$) and lower ($S < 0$) halves of the channel, respectively. Both non-symmetric solutions, when they appear, are stable, and the actual occurrence of one or the other solution depends on the initial conditions.

Obviously, for any $G > 0$ the symmetric solution with $S = 0$, stable for $m < m_c$ and unstable for $m > m_c$, ceases to exist. It can be seen in Fig. 1 that with a gradual increase in G, the symmetric solution turns into a solution with $S > 0$ at $m < m_c$, as it would be expected given the direction of the buoyancy forces. At the same time, for $m > m_c$, one of the asymmetric solutions (the "up" solution) also evolves into a solution with larger values of S. Thus, at $m < m_c$ the degree of asymmetry given by the parameter S increases gradually with G and for $m > m_c$ the inherent asymmetry of the flame, which also occurs in the absence of gravity, also increases. We can conclude that two mechanisms can be distinguished for the appearance of nonsymmetric flames during their propagation in the channel. The first is the mechanism caused by buoyancy forces. The second mechanism is determined by the action of the intrinsic flame instability during its propagation in the channel, as was pointed out in [13].

An interesting question arises. What happens to the other mirror "down" solution having $S < 0$ with a gradual increase in the parameter G ? Numerical calculations reveal that this solution solution does not disappear, and "down" non-symmetric flames exist for $G \geq 0$. These solutions can be obtained by the method described above, but only up to a certain point, $m = m_G$, indicated by open triangles in Fig. 1.

It should be noted that the solution emerging from the purely symmetric ($S = 0$) solution for $G = 0$ could not be obtained for $m > m_c$ by applying gradually increasing values of G, at least by the method used in the present study. Indeed, for $G = 0$ and $m > m_c$, the symmetric solution is obtained only by calculating in half of the channel, $0 < y < 1/2$, imposing the symmetry conditions at its center. When using these distributions for computations in a full channel, $0 < y < 1$, it switches to one of the nonsymmetric solutions. However, when $G > 0$, the calculations should be carried out only in the full channel, which explains the difficulties in calculating this solution which is intermediate between the "down" and "up" ones. However, it is obvious that this solution exists for $m > m_G$, at least as a mathematical object. The corresponding curves are supplemented (as a conjection) using dashed lines in Fig. 1 (left) for the curves with $G > 0$.

Figure 2 illustrates the dependence of the symmetry index S on the gravitational parameter G at the values of the flow rate fixed at $m = 1$ and 2 plotted for $Le = 1$. Remember, that for "up" and "down" solutions we have $S > 0$ and $S < 0$, respectively. The branches corresponding to the intermediate solution are shown by the dashed lines.

Therefore, according to the present calculations, in addition to the "up" solutions, stable "down" solutions (see below) exist in the presence of gravity for certain values of the parameters. In particular, for each G value, there is a critical value of the flow rate, $m = m_G$, above which two non-symmetric solutions can be obtained. Numerical results also showed that $m_G > m_c$ in the considered cases. Thus, the presence of buoyancy forces does not inhibit the existence of two non-symmetric solutions. It is also important to pay attention to the noticeable differences in the flash back points (the points with $u_f = 0$) for "up" and "down" solutions, which is important for safety problems.

An example of the temperature distributions and stream function isolines for the two solutions, "up" and "down", is illustrated in Fig. 3 for $m = 1$ and $G = 0.5$. It can be seen in this figure that for the "down" solution, the hotter gas continues to be located near the bottom of the channel, in contrast to

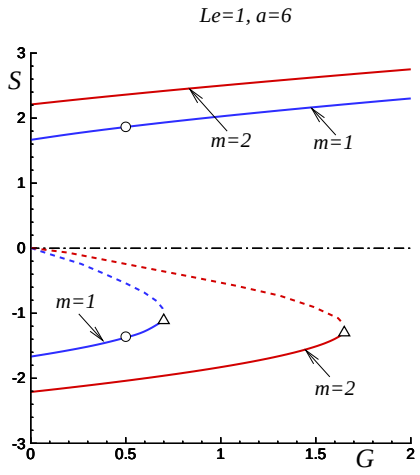

Fig. 2: Symmetry index as a function of the gravitational parameter, plotted for $Le = 1$ and two values of the flow rate $m = 1$ and 2. The dashed lines show the intermediate (not calculated) branch of the solution, which is generated from the symmetric solution at $G > 0$. The open circles on the curves with $m = 1$ correspond to the temperature distributions illustrated in Fig. 3.

intuitive notions of buoyancy.

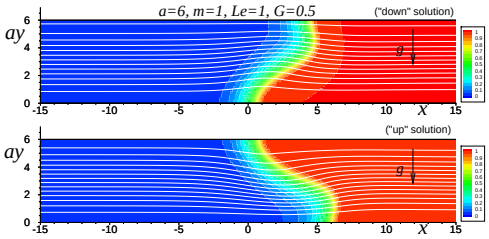

Fig. 3: Flame structure for "down" and "up" flames with hotter regions located in the lower and upper halves of the channel illustrated with color isotherms for the temperature field, for $a = 6$, $m = 1$ and $G = 0.5$. Thin white lines indicate streamlines. The distributions correspond to the points marked with open circles in Fig. 2.

4.2. Time-dependent simulations

The fact that the "down" solutions obtained above are stable over time was verified using time dependent calculations. As mentioned in Section 3, these calculations were carried out using two completely independent codes which provided very similar results.

Initial conditions for these time-dependent simulations were established from the stable "down" non-symmetric solutions obtained for $G = 0$. Figure 4 shows an example of the time history calculated with

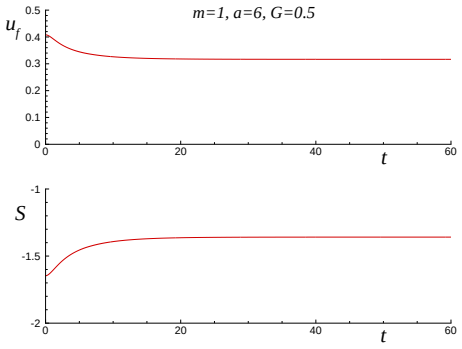

Fig. 4: An example of the time history for a "down" solution confirming the stability of this type of solutions, for $a = 6$ $m = 1$ and $G = 0.5$. The value of m is greater than the critical value m_G.

$G = 0.5$ for the flow rate $m = 1$, which is greater than m_G. The upper plot gives u_f as a function of time and the lower one shows the dynamics of the symmetry index S. It is seen that after the transition period, a steady-state is established corresponding to the solution branch "down" ($S < 0$).

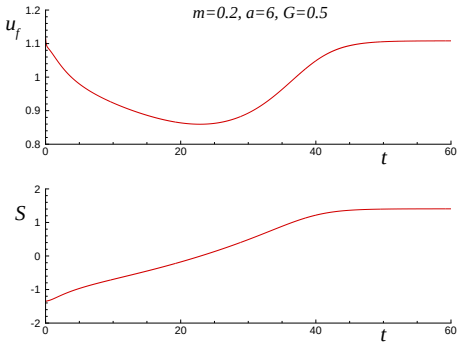

Fig. 5: An example of a time history for a flame with $a = 6$, $G = 0.5$ and $m = 0.2$, when the "down" solution evolves into the "up" solution from the $G = 0$ solution "down" initially.

Figure 5 illustrates the dynamics in which initial conditions correspond to a "down" flame with $G = 0$ and $m = 0.2$ (less than m_G), as the value of G is changed to $G = 0.5$. It can be seen that after some time interval the symmetry index S changes sign, that is, the structure of the flame switches from the "down" to the "up" state. The points corresponding to the final states obtained from time-dependent simulations for the above cases are shown in Fig. 1 by filled circles. From the results of Fig. 4 and Fig. 5 it is obvious that for $G = 0.5$ and $m = 1$ the "down" flame is stable while for $G = 0.5$ and $m = 0.2$ it is unstable. The "up" solutions corresponding to $G = 0.5$ and $m =$

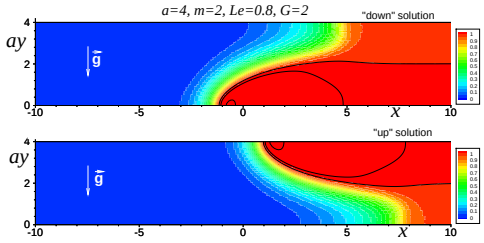

Fig. 6: Flame structure for "down" and "up" flames with hotter regions located in the lower and upper halves of the channel illustrated with color isotherms for the temperature field, for $a = 4$, $m = 2$ and $G = 2$. The temperature contours $\theta = 1$, 1.05, and 1.1 are shown by solid lines. The distributions correspond to the points marked with open circles in Fig. 7.

0.2 and 1 are both stable.

4.3. Influence of the Lewis number

The results presented above were obtained for a Lewis number equal to one. As shown in [13] for $G = 0$, the diffusive-thermal effect has a noticeable impact on the formation of nonsymmetric flames during their propagation in channels. For $Le < 1$ flames the critical flow rate and the critical channel width above which non-symmetric flames appear decrease in comparison with $Le = 1$ flames. This is linked to the high temperature regions appearing immediately after the combustion front at low Lewis numbers. An example of the temperature distributions for the "down" and "up" solutions is shown in Fig. 6 for $a = 4$ and $Le = 0.8$, where contours with temperatures above the adiabatic temperature are drawn with solid lines.

Figure 7 shows the dependence of the symmetry index S (left figure) and flame velocity u_f (right figure) on the flow rate m calculated for $a = 4$ and $Le = 0.8$. It can be seen that even such a small change in the Lewis number affects significantly these dependencies. It should also be noted that for $G = 0$, the curve representing the branch of nonsymmetric solutions does not touch the curve calculated for purely symmetric solutions. This behavior was also noted in [13]. This means that the m_G values indicated in Fig. 7 with open triangles are smaller than the corresponding bifurcation points m_c (marked with an open circle in Fig. 5). The similar behavior takes place for all curves with $G \geq 0$. In other words, subcritical bifurcation of solutions is observed, although it is impossible to calculate the exact value of the bifurcation point.

5. Conclusions

If gravitational, or buoyancy, forces acting across the channel are taken into account, a flame propagating in a horizontal channel cannot be absolutely symmetrical relative to its middle horizontal axis. An intuitive analysis could bring the reader to the conclusion that the flame should adopt a shape in which hot gases are concentrated in the upper part of the channel, due to the action of buoyancy forces. The results obtained in the present work show that this is not always the case.

The reason for this phenomenon lies in the fact that the flame experiences internal instabilities when it propagates in the channel. These instabilities can be of a diffusive-thermal nature or a purely hydrodynamic, Darrieus-Landau, character. In the first case, they can manifest even within the framework of the constant density model and appear as $Le < 1$. The second type of instability is possible in flames even with unity Lewis number. In both cases, the action of these instabilities can lead to the loss of symmetry of the flame, which also implies a change in propagation speed. In a horizontal two-dimensional channel, two non-symmetric flame types appear, with hot gases in the upper and lower halves of the channel.

In an analysis with no gravity effects, these two flames would mirror each other along the channel mid axis. If we imagine the gradual inclusion of the gravity field into consideration, the situation does not change abruptly: at least some part of the branch with a hotter region located near the channel bottom should continue to exist. The numerical simulations presented in this study confirm this.

In a recent work by the authors [13] carried out without taking into account the gravity effect, it was shown that a decrease in the Lewis number below unity leads to the appearance of non-symmetrical flames in narrower channels (for the same mass flow rate). In addition, the present numerical simulations prove that a decrease in the Lewis number also favors the existence of "up" and "down" flames, namely, this phenomenon can be observed in narrower channels than when $Le = 1$. On the other hand, taking into account thermal losses to the channel walls (not considered in the current study) will undoubtedly enhance the stability of symmetrical flames, as it was shown when modeling flames in the absence of gravitational forces [13].

Another, perhaps more important, conclusion from the presented analysis is that for slow flames, the buoyancy forces pushing hot gases upward is the leading mechanism in the formation of nonsymmetric flame shapes. This follows from the fact that the gravitational parameter, which is inversely proportional to the cube of the planar flame propagation speed for a given mixture, $G \sim S_L^{-3}$, is still large enough. However, for fast flames, characterized by a high planar flame speed, this parameter becomes rapidly small with increasing values of S_L. In these cases, the effect responsible for the appearance of nonsymmetric flame shapes is rather the intrinsic flame instabilities.

Acknowledgments

This work was financed by project #PID2019-

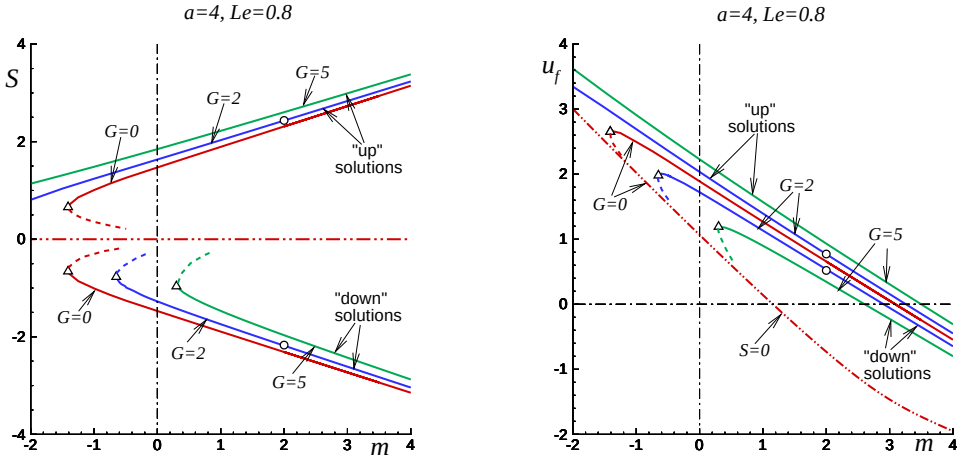

Fig. 7: Symmetry index S (left plot) and flame velocity relative to the channel walls u_f (right plot) for $G = 0$, 2 and 5 as functions of flow rate m; all curves for $a = 4$, $Le = 0.8$, $\beta = 10$ and $q = 5$. The dash-dot-dot curve shows the symmetrical solution computed in a half-width domain. The dashed lines show the intermediate (not calculated) branch of the solution, which is generated from the symmetric solution with increasing values of G. The open circles on the curves with $G = 2$ correspond to the temperature distributions shown in Fig. 6 for "up" and "down" solutions.

108592RB-C41,42,43 MCIN / AEI / 10.13039/ 501100011033.

References

[1] S.T. Lee, J.S. Tien, A numerical analysis of flame flashback in a premixed laminar system, *Combust. Flame* 48 (1982) 273-285.

[2] S.T. Lee, C.H. Tsai, Numerical investigation of steady laminar flame propagation in a circular tube, *Combust. Flame* 99 (1994) 484-490.

[3] C.L. Hackert, J.L. Ellzey, O.A. Ezekoye, Effects of thermal boundary conditions on flame shape and quenching in ducts, *Combust. Flame* 112 (1998) 73-84.

[4] J. Daou, M. Matalon, Flame propagation in Poiseuille flow under adiabatic conditions, *Combust. Flame* 124 (2001) 337-349 .

[5] V.N. Kurdyumov, E. Fernández-Tarrazo , Lewis number effect on the propagation of premixed laminar flames in narrow open ducts, *Combust. Flame* 128 (2002) 382394.

[6] J. Daou , M. Matalon, Influence of conductive heat-losses on the propagation of premixed flames in channels, *Combust. Flame* 128 (2002) 321-339.

[7] C. Cui, M. Matalon, J. Daou, J. Dold, Effects of differential diffusion on thin and thick flames propagating in channels, *Combust. Theory Model.* 8 (2004) 41-64.

[8] C. Cui , M. Matalon , T. Jackson, Pulsating mode of flame propagation in two-dimensional channels, *AIAA J.* 4 (2005) 12841292 .

[9] C. H. Tsai, The asymmetric behavior of steady laminar flame propagation in ducts, *Combust. Sci. Tech.* 180 (2008) 533–545.

[10] V. Kurdyumov, C. Jiménez, Propagation of symmetric and non-symmetric premixed flames in narrow channels: influence of conductive heat-losses, *Combust. Flame* 161 (2014) 927–936.

[11] V.N. Kurdyumov, C, Jiménez, Propagation of symmetric and non-symmetric lean hydrogen-air flames in narrow channels: Influence of heat losses, *Proc. Combust. Int.* 36 (2017) 1559-1567.

[12] K. Bioche, L. Vervisch, G. Ribert, Premixed fame-wall interaction in a narrow channel: impact of wall thermal conductivity and heat losses, *J. Fluid Mech.* 856 (2018) 5-35.

[13] A. Dejoan, C. Jiménez, V.N. Kurdyumov, Critical conditions for non-symmetric flame propagation in narrow channels: Influence of the flow rate, the thermal expansion, the Lewis number and heat-losses, *Combust. Flame* 209 (2019) 430-440.

[14] V. N. Kurdyumov, Lewis number effect on the propagation of premixed flames in narrow adiabatic channels: Symmetric and non-symmetric flames and their linear stability analysis, *Combust. Flame* 158 (2011) 1307–1317.

[15] D. Fernández-Galisteo, C. Jiménez, M. Sánchez-Sanz, V.N. Kurdyumov, The differential diffusion effect of the intermediate species on the stability of premixed flames propagating in microchannels, *Combust. Theory Model.* 18 (2014) 582–605.

[16] C. Jiménez, D. Fernández-Galisteo, V.N. Kurdyumov, DNS study of the propagation and flashback conditions of lean hydrogen-air flames in narrow channels: Symmetric and non-symmetric solutions, *Int. J. Hydrogen Energy* 40 (2015) 12541–12549.

[17] V.N. Kurdyumov, C, Jiménez, Structure and stability of premixed flames propagating in narrow channels of circular cross-section: Non-axisymmetric, pulsating and rotating flames, *Combust. Flame* 167 (2016) 149–163.

[18] A. Dejoan, V.N. Kurdyumov, Thermal expansion effect on the propagation of premixed flames in narrow channels of circular cross-section: Multiplicity of solutions, axisymmetry and non-axisymmetry., *Proc. Combust. Inst.* 37 (2019) 1927–1935.

[19] A. Dejoan, V.N. Kurdyumov, Three-dimensional simulations of isobaric premixed flames freely propagating in narrow circular channels: breaking of symmetry, *Combust. Theory. Modell.* 25 (2021) 1352-1374.

[20] K. Bioche, A. Pieyre, G. Ribert, F. Richecoeur, L. Vervisch, The role of gravity in the asymmetry of flames in narrow combustion chambers, *Combust. Flame* 203 (2019)

[21] T. Poinsot and D. Veynante, S. Candel, Quenching processes and premixed turbulent combustion diagrams,*J. Fluid Mech.*, 228 (1991) 561-606.

[22] http://www.openfoam.com.